IEEE Access
Multidisciplinary | Rapid Review | Open Access Journal

Received March 10, 2019, accepted March 21, 2019, date of publication March 25, 2019, date of current version April 12, 2019.

Digital Object Identifier 10.1109/ACCESS.2019.2907326

Performance Analysis and Improvement for VAMP Soft Frequency-Domain Equalizers

DONG LI[1,2], YANBO WU[1,3,5], JUN TAO[4,5,6], (Member, IEEE), AND MIN ZHU[1,3,5]

[1]Ocean Acoustic Technology Center, Institute of Acoustics, Chinese Academy of Sciences, Beijing 100190, China
[2]University of Chinese Academy of Sciences, Beijing 100190, China
[3]Beijing Engineering Technology Research Center of Ocean Acoustic Equipment, Beijing 100190, China
[4]Key Laboratory of Underwater Acoustic Signal Processing of Ministry of Education, School of Information Science and Engineering, Southeast University, Nanjing 210096, China
[5]State Key Laboratory of Acoustics, Chinese Academy of Sciences, Beijing 100190, China
[6]Acoustic Science and Technology Laboratory, Harbin Engineering University, Harbin 150001, China

Corresponding author: Yanbo Wu (wuyanbo@mail.ioa.ac.cn)

This work was supported in part by the National Natural Science Foundation of China under Grant 61471351 and Grant 61871114, in part by the National Key Research and Development Program of China under Grant 2016YFC0300300, in part by the Open Funds of State Key Laboratory of Acoustics, Chinese Academy of Sciences, under Grant SKLA201805, and in part by the Stable Supporting Fund of Acoustic Science and Technology Laboratory, Harbin Engineering University, under Grant SSJSWDZC2018013.

ABSTRACT The vector approximate message passing (VAMP) soft frequency-domain equalizer (SFDE) has been proposed for turbo equalization. It consists of an inner soft equalizer (ISE) and an inner soft slicer (ISS), which iteratively exchange block-wise extrinsic information to improve the equalization performance, analogous to the outer turbo iteration between a soft equalizer and a soft decoder. However, a comparison of the VAMP-SFDE with other types of self-iterative SFDEs, including the self-iterative block-wise soft interference cancellation (SI-BSIC) SFDE and the generalized approximate message passing (GAMP) SFDE, is lacking. Moreover, comprehensive performance analysis for the VAMP-SFDE is yet to be performed. In this paper, relations among the VAMP-SFDE, the SI-BSIC-SFDE, and the GAMP-SFDE are first revealed. After that, the performance analysis is provided for the VAMP-SFDE and it leads to an improved semi-adaptive damping (SAD) scheme for maintaining the *independence* between the ISS and ISE. The resulting SAD-VAMP-SFDE shows improved mean square error (MSE) evolution curves compared with the original VAMP-SFDE. The SAD-VAMP-SFDE-based turbo equalization outperforms those using the SI-BSIC-SFDE or GAMP-SFDE and approaches the matched filter bound (MFB) over low signal-to-noise ratio region. To further demonstrate its superiority, the SAD-VAMP-SFDE is employed to enable a near-capacity transceiver design, which adopts the serial concatenation of an irregular convolutional code and a unity-rate code on the transmitter side.

INDEX TERMS Frequency-domain turbo equalization, self-iterative soft equalizer (SISE), state evolution, vector approximate message passing (VAMP).

I. INTRODUCTION

Turbo equalization is a well-known receiver technique for combating the inter-symbol interference (ISI) [1]. It generally consists of a soft-input soft-output (SISO) equalizer and an SISO decoder, which iteratively exchange extrinsic information to improve the detection performance. For a given channel coding scheme, the soft equalizer determines the performance of the turbo equalization. The maximum *a posterior* (MAP) [2] or the minimum mean square error (MMSE) soft equalizers are optimal, in the sense that they glean as much information about transmitted symbols as possible based on the received signal and the *a priori* information from the soft decoder. Even though, both schemes are impractical in complexity for high-order modulations and/or long multipath channels.

In [3], a low-complexity soft equalizer was designed with the idea of soft interference cancellation (SIC) followed by linear filtering. It is essentially a linear minimum mean square error (LMMSE) equalizer with the *a priori* knowledge about equalized symbols available [4]. The initial SIC scheme [3]–[6] employing the *a priori* information from

The associate editor coordinating the review of this manuscript and approving it for publication was Donatella Darsena.

the decoder has been named the SIC-I, and it has been improved by the SIC-II and SIC-III [7]. The SIC-II simultaneously utilizes the *a priori* information of undetected symbols and the *a posterior* information of detected symbols for soft interference construction, as the equalization progresses [8], [9]. Because the *a posterior* decision generally has a higher fidelity than the *a priori* decision, the SIC-II leads to a better equalization performance than that of the SIC-I. The SIC-III is similar to the SIC-II, except that the *a posterior* decisions are fed back in a block-wise fashion. It achieves a better complexity-performance tradeoff than the SIC-II and is a special case of the more general self-iterative block-wise SIC (SI-BSIC) scheme [10], [11], for which the *a posterior* decision feedback is repeated multiple times to achieve incremental gain.

Despite enhanced SIC schemes, the aforementioned LMMSE soft equalizer is in general suboptimal due to its linear constraint, and there is still a performance gap from an optimal MMSE soft equalizer. To narrow the performance gap while maintain a reasonable complexity, approximate Bayesian methods have been adopted to design soft equalizers in the last decade. The approximate message passing (AMP) [12], [13] and the generalized AMP (GAMP) [14], [15] are two typical examples. Both methods are self-iterative in nature and to decouple the information exchanged over self-iterations, an Onsager correction [12], [16] is introduced. Their self-iterative behavior is characterized by a state evolution (SE) curve [14], [16]. The GAMP has been employed to implement a soft frequency-domain equalizer (SFDE) [17]–[20]. The original (G)AMP algorithm assumes a large mixing matrix with independent identically distributed (i.i.d.) Gaussian entries [14], [16], which may not be satisfied for an equalization problem. In order to overcome the limitation of AMP and accommodate general matrices, improved algorithms including the unitary transformation-based AMP (UT-AMP) [21], the vector AMP (VAMP) [22], [23] and the orthogonal AMP (OAMP) [24], have recently been proposed. The VAMP and OAMP belong to expectation propagation (EP)-type algorithms [25], which have enabled many iterative receivers [26]–[31]. In particular, a VAMP-SFDE has been proposed in [28].

The VAMP-SFDE, however, was not thoroughly investigated. First, the connection between the VAMP-SFDE and other self-iterative SFDEs including the SI-BSIC-SFDE and GAMP-SFDE, is yet to be revealed. Second, because practical channel matrices may not be Gaussian and right-rotationally invariant, effectiveness of the SE prediction as well as convergence performance for the VAMP-SFDE remains unclear. By addressing aforementioned questions, this paper makes the following contributions:

- First, relations among the VAMP-SFDE, GAMP-SFDE [17], and SI-BSIC-SFDE, are revealed. It shows the SI-BSIC-SFDE is a simplified variant of the VAMP-SFDE and the GAMP-SFDE has a similar mechanism to the VAMP-SFDE except for the Onsager correction. In terms of complexity, the three SISEs are comparable.
- Second, the SE analysis is performed for the VAMP-SFDE, and it leads to a semi-adaptive damping (SAD) scheme for improving the convergence and robustness of the VAMP-SFDE. The performance of the resulting VAMP-SFDE with SAD, named SAD-VAMP-SFDE hereafter, is then evaluated within turbo equalization. Both extrinsic information transfer (EXIT) and bit error rate (BER) results show the SAD-VAMP-SFDE outperforms the GAMP-SFDE and the SI-BSIC-SFDE.
- Third, a transmission scheme adopting the SAD-VAMP-SFDE based turbo equalization is designed. It introduces a unity-rate code (URC) precoding in addition to the channel coding. The channel encoder is an irregular convolutional code (IrCC) [32], designed by matching the EXIT curve of the concatenation of the SAD-VAMP-SFDE and URC decoder. Such a transmitter design leads to a turbo equalization with three-fold iterative processing on the receiver side. The overall performance of the proposed transmission system is only 1.3 dB from the optimal performance under severe ISI channels.

The rest of this paper is organized as follows. In Section II, the system model for a single-carrier block transmission is introduced, followed by a revisit of the VAMP-SFDE and a comparison among the VAMP-SFDE, SI-BSIC-SFDE, and GAMP-SFDE. In Section III, an SE analysis of the VAMP-SFDE leading to the SAD scheme is first presented. Afterwards, the performance of the resulting SAD-VAMP-SFDE is extensively investigated via numerical simulations. Section IV demonstrates a transmission system design using the SAD-VAMP-SFDE based turbo equalization, and Section V concludes the paper.

Notations: The $(\cdot)^{\mathsf{T}}$ and $(\cdot)^{\mathsf{H}}$ denote the transpose and Hermitian, respectively. The $\mathbb{E}(\cdot)$ and $\mathrm{Var}(\cdot)$ take the expectation and variance operations. For a matrix $\mathbf{A}$, $[\mathbf{A}]_{ij}$ represents the j-th element of the i-th row. For a vector $\mathbf{x}$, $[\mathbf{x}]_i$ represents its i-th element, $\mathrm{Diag}(\mathbf{x})$ returns a diagonal matrix with diagonal elements given by $\mathbf{x}$. A complex Gaussian vector $\mathbf{x} \in \mathbb{C}^N$ with a mean $\mathbf{m}$ and a covariance matrix $\mathbf{C}$ is denoted as $\mathbf{x} \sim \mathcal{CN}(\mathbf{m}, \mathbf{C})$. The $\mathbf{I}$ is an identity matrix of proper size.

II. SYSTEM MODEL AND THE VAMP-SFDE

A single-carrier block transmission with cyclic prefix (CP) is considered. At the transmitter, an information bit sequence is encoded, interleaved, then grouped into size-M tuples $\{\mathbf{c}_n\}$. The tuple $\mathbf{c}_n = [c_n^1 \; c_n^2 \; \ldots \; c_n^M]$, is mapped to a symbol x_n taken from a 2^M-ary constellation $\mathcal{M} = \{\alpha_1, \alpha_2, \ldots, \alpha_{2^M}\}$.

At the receiver, the received time-domain signal over one block is given as

$$y_n = \sum_{i=0}^{L-1} h_i x_{n-i} + w_n \quad n = 0, 1, \ldots, N-1, \tag{1}$$

where $\mathbf{h} = [h_0, h_1, \ldots, h_{L-1}]^{\mathsf{T}}$ denotes the channel impulse response (CIR), w_n represents a complex additive white Gaussian noise (AWGN) sample, and N is the block size. Define $\mathbf{y} = [y_0, y_1, \ldots, y_{N-1}]^{\mathsf{T}} \in \mathbb{C}^N$,

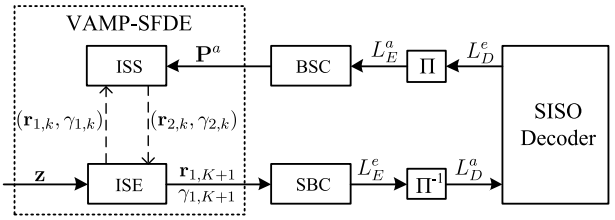

FIGURE 1. Block diagram of VAMP-SFDE based turbo equalization system (the BSC is a bit-to-symbol convertor translating the *a priori* bit LLRs L_E^a into the *a priori* symbol probabilities $\mathbf{P}^a$, and the SBC is a symbol-to-bit convertor translating the extrinsic mean-vector $\mathbf{r}_{1,K+1}$ and average-variance $\gamma_{1,K+1}^{-1}$ into extrinsic bit LLRs L_E^e).

$\mathbf{x} = [x_0, x_1, \ldots, x_{N-1}]^{\mathsf{T}} \in \mathcal{M}^N$, $\mathbf{H} \in \mathbb{C}^{N\times N}$ as the channel matrix based on the CIR $\mathbf{h}$, and $\mathbf{w} = [w_0, w_1, \ldots, w_{N-1}]^{\mathsf{T}} \in \mathbb{C}^N \sim \mathcal{CN}(\mathbf{0}, \gamma_w^{-1}\mathbf{I})$, the system model in matrix form is then

$$\mathbf{y} = \mathbf{H}\mathbf{x} + \mathbf{w}. \tag{2}$$

Due to the CP, for which $x_{-1}, x_{-2}, \ldots, x_{-L_{\text{cp}}}$ is a copy of $x_{N-1}, x_{N-2}, \ldots, x_{N-L_{\text{cp}}}$ with $L_{\text{cp}} \geq L-1$, the channel matrix $\mathbf{H}$ becomes circulant and it can be decomposed as $\mathbf{H} = \mathbf{F}^{\mathsf{H}}\mathbf{S}\mathbf{F}$, with $\mathbf{F}$ being a discrete Fourier transform (DFT) matrix with $[\mathbf{F}]_{mn} = (1/\sqrt{N})\exp(-j2\pi mn/N)$, and $\mathbf{S} = \text{Diag}(\mathbf{s})$ with $\mathbf{s} = \sqrt{N}\mathbf{F}\mathbf{h} = [s_0, s_1, \ldots, s_{N-1}]^{\mathsf{T}}$. Applying the DFT matrix on both sides of (2) as in [17], one obtains the following frequency-domain model

$$\mathbf{z} = \mathbf{S}\mathbf{F}\mathbf{x} + \mathbf{w}', \tag{3}$$

where $\mathbf{z} = \mathbf{F}\mathbf{y}$, and it is easy to verify $\mathbf{w}' = \mathbf{F}\mathbf{w}$ obeys the same distribution as $\mathbf{w}$. Based on (3), the VAMP-SFDE is revisited and compared with other self-iterative SFDEs.

A. THE VAMP-SFDE REVISIT

In Fig. 1, a turbo equalization scheme adopting the VAMP-SFDE [28] is shown. From the figure, the VAMP-SFDE consists of an inner soft equalizer (ISE) and an inner soft slicer (ISS). For the ISS, its input *a priori* symbol probabilities, $P^a(x_n = \alpha_i)$, are computed by the BSC with the *a priori* bit log-likelihood-ratios (LLRs), $L_E^a(c_n^q)$, coming from the SISO decoder as

$$P^a(x_n = \alpha_i) = \prod_{q=1}^{M} \frac{1 + (1-2a_i^q)\tanh(L_E^a(c_n^q)/2)}{2}, \tag{4}$$

where the symbol α_i maps to a size-M bit tuple $\mathbf{a}_i = [a_i^1\ a_i^2\ \ldots\ a_i^M]$. The $P^a(x_n = \alpha_i)$ together with the extrinsic mean vector $\mathbf{r}_{1,k}$ and average variance $\gamma_{1,k}^{-1}$ from the ISE are used to compute the *a posterior* symbol probability, $P(x_n = \alpha_i)$, based on which the *a posterior* mean-vector $\widehat{\mathbf{x}}_{1,k}$ and the average variance $\eta_{1,k}^{-1}$ of $\mathbf{x}$ are conveniently obtained. After that, the output of the ISS is obtained by applying the Onsager correction as

$$\gamma_{2,k} = \eta_{1,k} - \gamma_{1,k} \tag{5a}$$

$$\mathbf{r}_{2,k} = \frac{\eta_{1,k}\widehat{\mathbf{x}}_{1,k} - \gamma_{1,k}\mathbf{r}_{1,k}}{\gamma_{2,k}}. \tag{5b}$$

The ISE is actually identical to the soft LMMSE equalizer with a concise derivation of the extrinsic information [6]. The *a posterior* mean-vector $\widehat{\mathbf{x}}_{2,k}$ of the ISE is computed as

$$\widehat{\mathbf{x}}_{2,k} = \mathbf{r}_{2,k} + \gamma_w \mathbf{F}^{\mathsf{H}}\mathbf{S}^{\mathsf{H}}\mathbf{D}_k(\mathbf{z} - \mathbf{S}\mathbf{F}\mathbf{r}_{2,k}), \tag{6}$$

where $\mathbf{D}_k$ is a diagonal matrix with its n-th diagonal element $(\gamma_w|s_n|^2 + \gamma_{2,k})^{-1}$. Based on $\widehat{\mathbf{x}}_{2,k}$ and $\eta_{2,k} = (\frac{1}{N}\sum_{n=1}^{N}[\mathbf{D}_k]_{nn})^{-1}$, the output of the ISE to the ISS is obtained as

$$\gamma_{1,k+1} = \eta_{2,k} - \gamma_{2,k} \tag{7a}$$

$$\mathbf{r}_{1,k+1} = \frac{\eta_{2,k}\widehat{\mathbf{x}}_{2,k} - \gamma_{2,k}\mathbf{r}_{2,k}}{\gamma_{1,k+1}}, \tag{7b}$$

where the Onsager correction is again applied. In the final K-th self-iteration, the ISE outputs the extrinsic mean-vector $\mathbf{r}_{1,K+1}$ and average variance $\gamma_{1,K+1}^{-1}$, with which the extrinsic bit LLRs are computed in the SBC unit as (8), as shown at the bottom of this page. The self-iteration of the VAMP-SFDE is summarized in Algorithm 1.

B. COMPARISON WITH OTHER SELF-ITERATIVE SFDEs

1) SI-BSIC-SFDE

For the SI-BSIC-SFDE derived from the SIC-III [7], the *a posterior* soft decisions are repeatedly fed back in a block-wise fashion. It is easy to verify the SI-BSIC-SFDE is equivalent to the VAMP-SFDE with $\gamma_{1,k} \equiv 0$, such that $\gamma_{2,k} = \eta_{1,k}$, $\mathbf{r}_{2,k} = \widehat{\mathbf{x}}_{1,k}$ in lines 4–5 of Algorithm 1. The ISS thus outputs the *a posterior* information instead of the extrinsic information over self iterations, and the final output $\mathbf{r}_{1,K+1}$ may not be independent of the initial input $\widehat{\mathbf{x}}_{1,0}$. In other words, the *independence constraint* is not met, which may affect the convergence of an SI-BSIC-SFDE based turbo equalization.

2) GAMP-SFDE

To facilitate the comparison with the VAMP-SFDE given in Algorithm 1, the ISE of original GAMP-SFDE [17] is purposely presented in the LMMSE form in Algorithm 2. It can be verified this alternative form of the GAMP-SFDE in Algorithm 2 is equivalent to that in [17]. Compare with the VAMP-SFDE, the GAMP-SFDE has no Onsager correction for the ISS. As to the ISE, the GAMP-SFDE introduces an

$$L_E^e(c_n^q) = \ln \frac{\sum_{\alpha_i: a_i^q = 0} \exp\left(-|[\mathbf{r}_{1,K+1}]_n - \alpha_i|^2\gamma_{1,K+1} - \sum_{q'\neq q} a_i^{q'} L_E^a(c_n^{q'})\right)}{\sum_{\alpha_i: a_i^q = 1} \exp\left(-|[\mathbf{r}_{1,K+1}]_n - \alpha_i|^2\gamma_{1,K+1} - \sum_{q'\neq q} a_i^{q'} L_E^a(c_n^{q'})\right)} \tag{8}$$

Algorithm 1 Self Iteration of the VAMP-SFDE

Require: $\mathbf{P}^a_{N\times 2^M}$, where $[\mathbf{P}^a]_{ni} = P^a(x_n = \alpha_i)$, $\mathbf{r}_{1,0} = \mathbf{0} \in \mathbb{C}^N$, $\gamma_{1,0} = 0$ and $\mathbf{H} = \mathbf{F}^{\mathsf{H}}\mathbf{S}\mathbf{F}$, $\mathbf{z}$.

1: **for** $k = 0 : K$ **do**

// Inner Soft Slicer (ISS)

2: $P_i = [\mathbf{P}^a]_{ni} \exp(-\gamma_{1,k}|\alpha_i - [\mathbf{r}_{1,k}]_n|^2)$

$P(x_n = \alpha_i) = \frac{P_i}{\sum_{m=1}^{2^M} P_m}$, $i = 1, 2, \ldots, 2^M$

$[\widehat{\mathbf{x}}_{1,k}]_n = \sum_{i=1}^{2^M} \alpha_i P(x_n = \alpha_i)$, $n = 0, 1, \ldots, N-1$

3: $\eta_{1,k} = \left(\frac{1}{N}\sum_{n=0}^{N-1} \mu_n\right)^{-1}$,

where $\mu_n = \sum_{i=1}^{2^M} |\alpha_i - [\widehat{\mathbf{x}}_{1,k}]_n|^2 P(x_n = \alpha_i)$

4: $\gamma_{2,k} = \eta_{1,k} - \gamma_{1,k}$

5: $\mathbf{r}_{2,k} = (\eta_{1,k}\widehat{\mathbf{x}}_{1,k} - \gamma_{1,k}\mathbf{r}_{1,k})/\gamma_{2,k}$

// Inner Soft Equalizer (ISE)

6: $\widehat{\mathbf{x}}_{2,k} = \mathbf{r}_{2,k} + \gamma_w \mathbf{F}^{\mathsf{H}}\mathbf{S}^{\mathsf{H}}\mathbf{D}_k(\mathbf{z} - \mathbf{S}\mathbf{F}\mathbf{r}_{2,k})$,

where $\mathbf{D}_k = \mathrm{Diag}\left(\{1/(\gamma_w|s_n|^2 + \gamma_{2,k})\}_{n=0}^{N-1}\right)$

7: $\eta_{2,k} = \left(\frac{1}{N}\sum_{n=0}^{N-1}[\mathbf{D}_k]_{nn}\right)^{-1}$

8: $\gamma_{1,k+1} = \eta_{2,k} - \gamma_{2,k}$

9: $\mathbf{r}_{1,k+1} = (\eta_{2,k}\widehat{\mathbf{x}}_{2,k} - \gamma_{2,k}\mathbf{r}_{2,k})/\gamma_{1,k+1}$

10: **end for**

11: **return** $\mathbf{r}_{1,K+1}$, $\gamma_{1,K+1}$

Algorithm 2 GAMP-SFDE in LMMSE Form

Require: $\mathbf{P}^a_{N\times 2^M}$, where $[\mathbf{P}^a]_{ni} = P^a(x_n = \alpha_i)$, $\mathbf{r}_0 = \mathbf{0} \in \mathbb{C}^N$, $\mathbf{e}_0 = \mathbf{0} \in \mathbb{C}^N$, $\gamma_0 = 0$, $\mathbf{H} = \mathbf{F}^{\mathsf{H}}\mathbf{S}\mathbf{F}$, $\mathbf{z}$.

1: **for** $k = 0 : K$ **do**

// Inner Soft Slicer (ISS)

2: $P_i = [\mathbf{P}^a]_{ni} \exp(-\gamma_k|\alpha_i - [\mathbf{r}_k]_n|^2)$

$P(x_n = \alpha_i) = \frac{P_i}{\sum_{m=1}^{2^M} P_m}$, $i = 1, 2, \ldots, 2^M$

$[\widehat{\mathbf{x}}_{1,k}]_n = \sum_{i=1}^{2^M} \alpha_i P(x_n = \alpha_i)$, $n = 0, 1, \ldots, N-1$

3: $\eta_{1,k} = \left(\frac{1}{N}\sum_{n=0}^{N-1} \mu_n\right)^{-1}$,

where $\mu_n = \sum_{i=1}^{2^M} |\alpha_i - [\widehat{\mathbf{x}}_{1,k}]_n|^2 P(x_n = \alpha_i)$

// Inner Soft Equalizer (ISE)

4: $\widehat{\mathbf{x}}_{2,k} = \widehat{\mathbf{x}}_{1,k} + \gamma_w \mathbf{F}^{\mathsf{H}}\mathbf{S}^{\mathsf{H}}\mathbf{D}_k(\mathbf{z} - \mathbf{S}\mathbf{F}\widehat{\mathbf{x}}_{1,k})$,

where $\mathbf{D}_k = \mathrm{Diag}\left(\{1/(\gamma_w|s_n|^2 + \eta_{1,k})\}_{n=0}^{N-1}\right)$

5: $\eta_{2,k} = \left(\frac{1}{N}\sum_{n=0}^{N-1}[\mathbf{D}_k]_{nn}\right)^{-1}$

6: $\gamma_{k+1} = (\eta_{2,k} - \eta_{1,k})\bar{\nu}_k$, where $\bar{\nu}_k = \eta_{1,k}/\eta_{2,k}$

7: $\mathbf{r}_{k+1} = (\eta_{2,k}\widehat{\mathbf{x}}_{2,k} - \eta_{1,k}\widehat{\mathbf{x}}_{1,k})/(\eta_{2,k} - \eta_{1,k}) +$
$\gamma_{k+1}^{-1}\mathbf{F}^{\mathsf{H}}\mathbf{S}^{\mathsf{H}}(\mathbf{I} - \boldsymbol{\nu}_k)\mathbf{e}_k$, where $\boldsymbol{\nu}_k = \eta_{1,k}\mathbf{D}_k$

8: $\mathbf{e}_{k+1} = \gamma_w(\mathbf{z} - \mathbf{S}\mathbf{F}\widehat{\mathbf{x}}_{2,k}) + (\mathbf{I} - \boldsymbol{\nu}_k)\mathbf{e}_k$

9: **end for**

10: **return** $\mathbf{r}_{K+1}$, γ_{K+1}

Onsager correction term, $\boldsymbol{g} = \gamma_{k+1}^{-1}\mathbf{F}^{\mathsf{H}}\mathbf{S}^{\mathsf{H}}(\mathbf{I} - \boldsymbol{\nu}_k)\mathbf{e}_k$, as seen in line 7 of Algorithm 2, where the $\mathbf{e}_k$ accounts for the equalization error $\mathbf{z} - \mathbf{S}\mathbf{F}\widehat{\mathbf{x}}_{2k}$ over all previous self-iterations (see line 8 in Algorithm 2). The GAMP-SFDE Onsager correction, however, is problematic under channels with severe frequency selectivity. In such cases, some diagonal elements of $\mathbf{S}$ defined after (2) thus $\mathbf{S}^{\mathsf{H}}(\mathbf{I} - \boldsymbol{\nu}_k)$ approach zero. As a result, the corresponding equalization errors in $\mathbf{e}_k$ cannot be effectively incorporated via the Onsager correction term $\boldsymbol{g}$. The GAMP-SFDE therefore reduces to the SI-BSIC-SFDE.

3) COMPLEXITY COMPARISON

A brief complexity comparison is performed for the VAMP-SFDE, the GAMP-SFDE [17], the LMMSE-SFDE obtained as the VAMP-SFDE with no inner iterations ($K = 0$), and the SI-BSIC-SFDE. A size-N FFT operation incurs $\frac{N}{2}\log_2 N$ complex multiplications (CMs), and the $\exp(\cdot)$ operation is calculated via a piecewise linear function. The incurred number of CMs and real multiplications (RMs) are compared in Table 1 for the aforementioned soft equalizers. It is clear the VAMP-SFDE, the GAMP-SFDE, and the SI-BSIC-SFDE are comparable in complexity.

III. PERFORMANCE ANALYSIS VIA NUMERICAL SIMULATIONS

A single-carrier block transmission system, which has a block size $N = 1024$ and a CP length $L_{\mathrm{cp}} = 10$, is considered. It employs a rate-1/2 recursive systemic convolutional (RSC) code with a generator polynomial $(3, 2)_8$ and the Log-MAP soft decoding [33].

A. SE ANALYSIS AND SEMI-ADAPTIVE DAMPING (SAD) SCHEME

The MSE evolution of the VAMP algorithm over self-iterations can be predicted by the SE equations [22], which are also applicable to the VAMP-SFDE and omitted here for brevity. According to [22], when the linear mixing matrix ($\mathbf{H}$ in (2) or $\mathbf{S}\mathbf{F}$ in (3)) is right-rotationally invariant, the predicted MSEs by the SE equation are pretty accurate. The MSE evolution of the VAMP-SFDE is next simulated and compared with the SE prediction under different channels, including the Proakis-A channel with coefficients [0.04, −0.05, 0.07, −0.21, −0.5, 0.72, 0.36, 0, 0.21, 0.03, 0.07], the minimum-distance path-6 (MD-6) channel [34] with coefficients

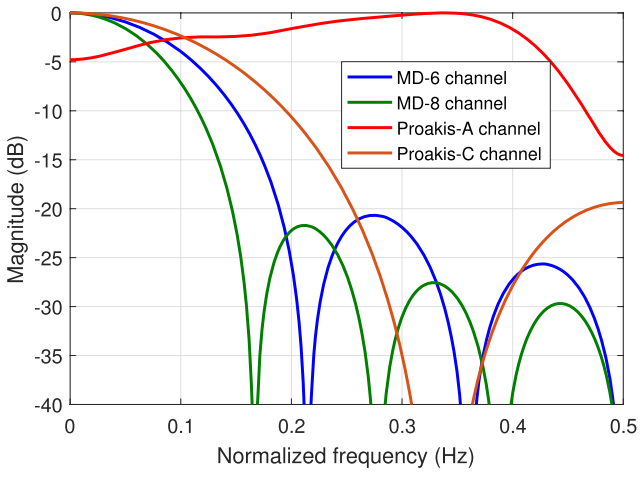

FIGURE 2. Amplitude-frequency responses of the Proakis-A channel, the MD-6 channel, and the MD-8 channel.

TABLE 1. Complexity comparison among the soft equalizers.

	CMs	RMs
LMMSE-SFDE	$2N + N\log_2 N + 2^M N$	$11N + 2^M N \cdot 2$
SI-BSIC-SFDE	$(2N + N\log_2 N + 2^M N \cdot 2) \cdot (K+1)$	$(11N + 2^M N \cdot 7) \cdot (K+1)$
GAMP-SFDE	$(3N + N\log_2 N + 2^M N \cdot 2) \cdot (K+1)$	$(9N + 2^M N \cdot 7) \cdot (K+1)$
VAMP-SFDE	$(2N + N\log_2 N + 2^M N \cdot 2) \cdot (K+1)$	$(15N + 2^M N \cdot 7) \cdot (K+1)$

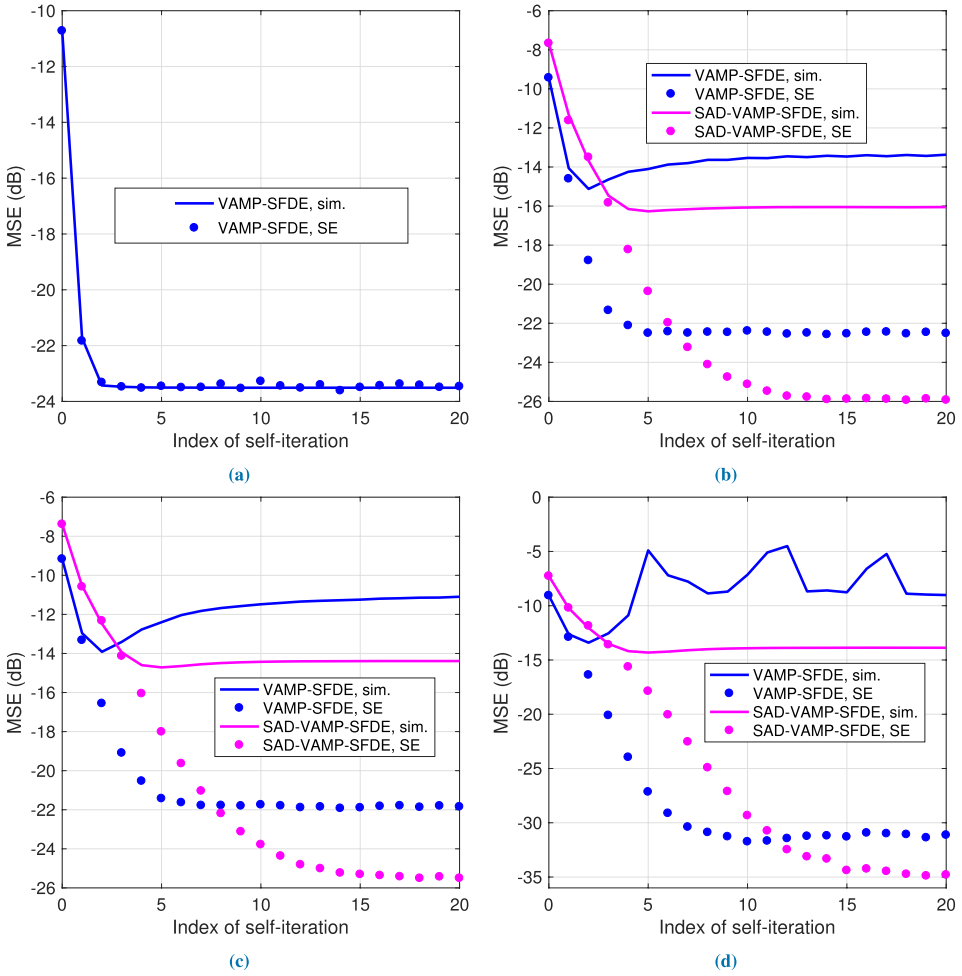

FIGURE 3. MSE evolutions of the VAMP-SFDE and SAD-VAMP-SFDE under (a) the Proakis-A channel with SNR = 8 dB, (b) the Proakis-C channel with SNR = 8 dB, (c) the MD-6 channel with SNR = 8 dB, and (d) the MD-8 channel with SNR = 10 dB.

[0.23, 0.42, 0.52, 0.52, 0.42, 0.23], the MD-8 channel with coefficients [0.16,0.30, 0.41, 0.46, 0.46, 0.40, 0.30, 0.16], and the Proakis-C channel with coefficients [0.227, 0.460 0.688, 0.460, 0.227]. The amplitude-frequency responses of the channels are shown in Fig. 2, where the MD-6, MD-8, and Proakis-C channels manifest severe frequency selectivity, The *a priori* LLRs of the VAMP-SFDE were artificially generated based on the *a priori* mutual information I_{in}^E set as 0.8 [35], [36]. The simulated MSE in the k-th self-iteration was calculated as $\text{MSE} = \mathbb{E}\left(\|\widehat{\mathbf{x}}_{2,k} - \mathbf{x}\|^2\right)$.

The results are shown in Fig. 3, where the blue curves corresponding to the VAMP-SFDE are discussed first. Under the mild Proakis-A channel, the simulated MSE curve of the VAMP-SFDE agrees very well with the predicted one, even though the underlying channel matrix $\mathbf{H}$ is not right-rotationally invariant. Under remaining channels with high frequency selectivity, however, the simulated MSEs deviate from the SE predictions and eventually diverge as the self-iteration continues.

For AMP-type algorithms, damping technique has proved to be an effective way to address the aforementioned divergence issue [37]–[39]. Herein, an improved damping setting is introduced for the VAMP-SFDE under severe channels. Specifically, lines 2 and 8 of Algorithm 1 are modified as

follows

$$[\widehat{\mathbf{x}}_{1,k}]_n = \theta\Big(\sum_{i=1}^{2^M}\alpha_i P(x_n=\alpha_i)\Big) + (1-\theta)[\widehat{\mathbf{x}}_{1,k-1}]_n \quad (9)$$

$$\gamma_{1,k+1} = \theta(\eta_{2,k}-\gamma_{2,k}) + (1-\theta)\gamma_{1,k}, \quad (10)$$

where $\theta \in (0,1]$ is a damping factor. A smaller θ corresponds to a larger damping and there is no damping if $\theta = 1$. It is difficult, if not impossible, to derive an optimal damping factor. Instead, one resorts to numerical solutions. In Fig. 4, MSEs of the VAMP-SFDE as functions of the damping factors are depicted under multiple channels. In the simulations, the number of self-iterations for the VAMP-SFDE was 4 and a QPSK modulation was adopted. From the figure, a good choice of the damping factor shall fall in the range of [0.65, 0.70], despite the channel conditions. Based on the observations, we propose a heuristic SAD scheme which adaptively selects the damping factor as follows

- Initialize a damping set: $\boldsymbol{\Theta} = \{0.65, 0.67, 0.70\}$, where an intermediate value, 0.67, is included in addition to the two end points;
- Define a cost function: $J(\theta) = \|\mathbf{z} - \mathbf{S}\mathbf{F}\widehat{\mathbf{x}}_{1,k}\|^2$, where $\widehat{\mathbf{x}}_{1,k}$ is from (9);
- Determine the optimal damping factor that minimizes the cost function as: $\theta^{\text{opt}} = \arg\min_{\theta\in\boldsymbol{\Theta}} J(\theta)$.

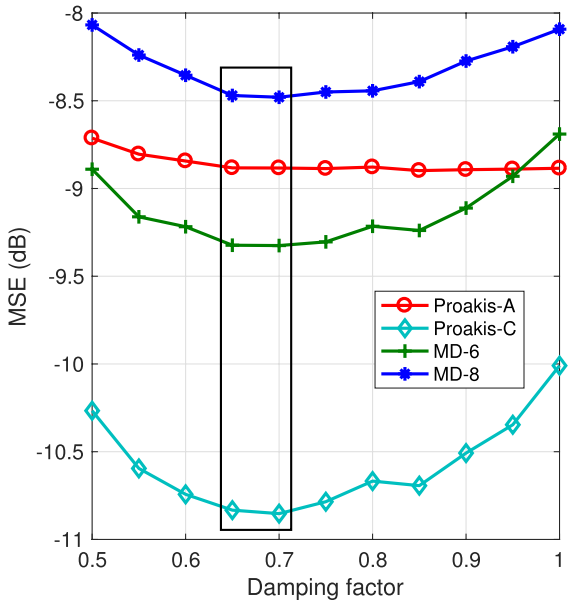

FIGURE 4. MSEs versus damping factor for the VAMP-SFDE with the fixed damping under different channels ($I_{\text{in}}^E = 0.6$, SNR = 2 dB for the Proakis-A channel, SNR = 8 dB for the Proakis-C and MD-6 channels, and SNR = 9 dB for the MD-8 channel).

The SE analysis for the SAD-VAMP-SFDE is shown in Fig. 3(b), 3(c) and 3(d). Compared with the VAMP-SFDE without damping, the SAD-VAMP-SFDE addresses the divergence issue, despite a decreased convergence speed. The simulated MSEs agree well with the SE predictions in initial 3–4 self-iterations, and stay constant afterwards. The reason is that the circulant channel matrix $\mathbf{H}$ does not meet the right-rotationally invariant requirement, leading to a short constraint length and thus limited iterative gain.

B. CONVERGENCE AND PERFORMANCE OF TURBO EQUALIZATION

In this subsection, we investigate the convergence and performance of four turbo equalization schemes employing the LMMSE-SFDE, the SI-BSIC-SFDE, the GAMP-SFDE, and the SAD-VAMP-SFDE, respectively.

1) CONVERGENCE INVESTIGATION

The EXIT chart is a powerful tool to investigate the convergence of turbo equalization [40]. When the *independence constraint* is met, it can predict the iterative trajectory and performance. However, a violation of the *independence constraint* will make the actual trajectory deviate from the predicted path [35], [41]. The satisfaction of the *independent constraint* of a soft equalizer can be measured by the correlation between its input *a priori* information and output *extrinsic* information [42]. Before the EXIT chart results are demonstrated, a numerical analysis on the correlation of the SISEs is first provided.

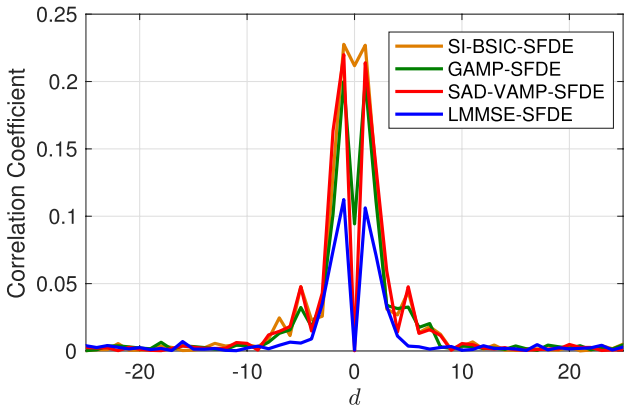

FIGURE 5. A comparison of correlation coefficients ρ_d among various soft equalizers under the MD-6 channel (BPSK modulation and SNR is 7dB).

In the simulation, BPSK modulation and the MD-6 channel were used and the SNR was 7 dB. At the receiver, the input *a priori* LLRs to the soft equalizer was artificially generated based on transmitted bits and noise variance [35]. The correlation values, ρ_d, between the output extrinsic LLR at position i and the input LLR at position $i+d$ were then computed. Simulation results are shown in Fig. 5, where the sample number of each Monte Carlo simulation was set to 3000 and the number of self-iterations was 4.

The correlation ρ_0 at $d = 0$ reflects the satisfaction of the *independent constraint*. As expected, $\rho_0 = 0$ for the LMMSE-SFDE as the *independent constraint* was completely met, whereas the SI-BSIC-SFDE has the largest ρ_0 value. The GAMP-SFDE produces a moderate ρ_0, with the

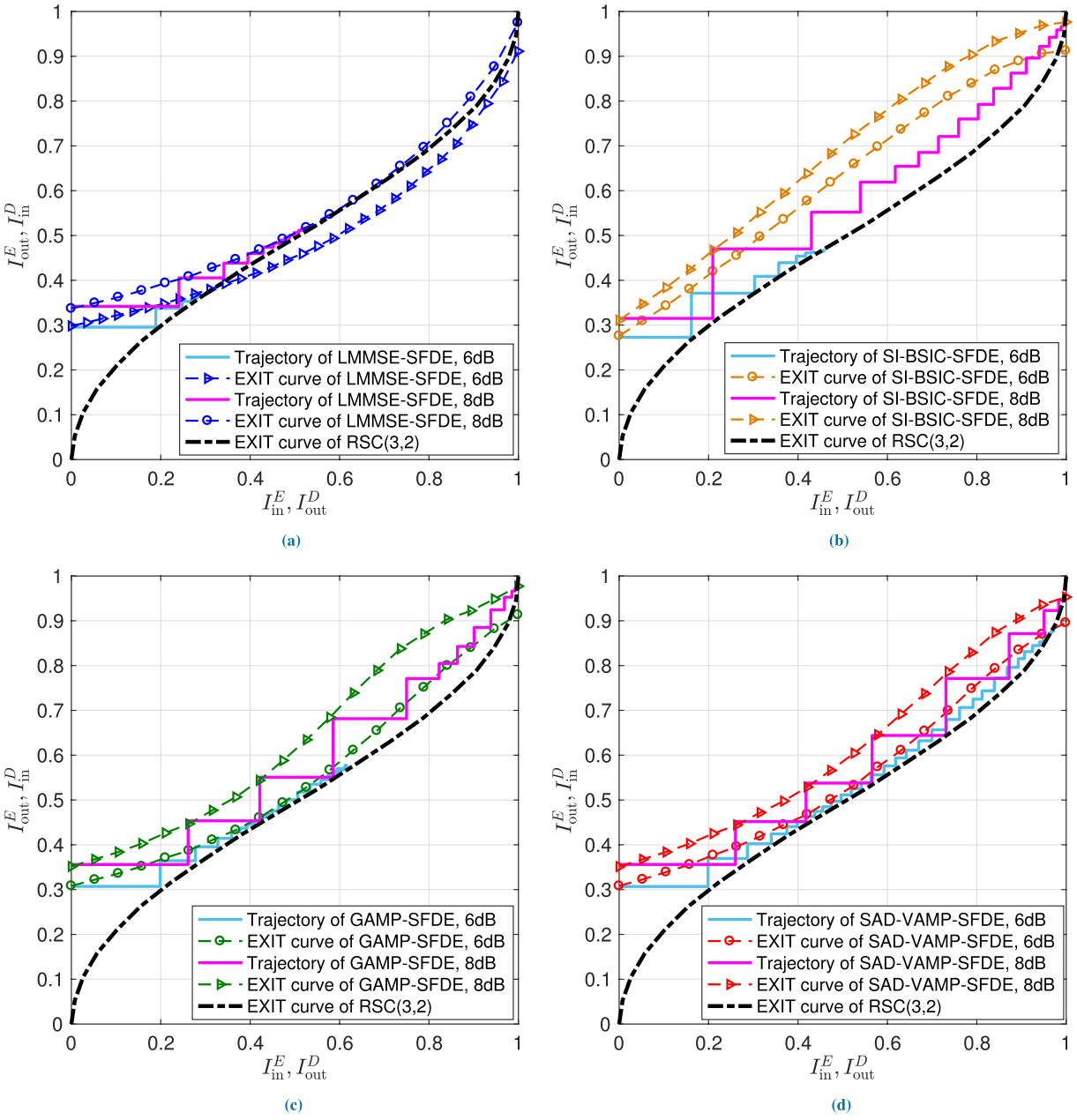

FIGURE 6. EXIT charts of four turbo equalization schemes based on the LMMSE-SFDE in (a), the SI-BSIC-SFDE in (b), the GAMP-SFDE in (c), and the SAD-VAMP-SFDE in (d), under different E_b/N_0 conditions.

help of Onsager correction. The ρ_0 of the SAD-VAMP-SFDE approaches zero, attributed to the proposed SAD scheme and Onsager corrections. The correlation ρ_d at $d \neq 0$ indicates the information of a given bit gleaned from its neighbors. Clearly, all three self-iterative SISEs outperform the LMMSE-SFDE in this regard.

Next, the EXIT chart results are presented in Fig. 6, where the MD-6 channel and QPSK modulation were adopted for simulations. Obviously, the trajectories of the LMMSE-SFDE and the SAD-VAMP-SFDE agree well with their EXIT curves regardless of E_b/N_0 (i.e. the SNR per bit) conditions, attributed to the satisfaction of the *independent constraint*. For the SI-BSIC-SFDE and GAMP-SFDE, however, their trajectories deviate from the EXIT curves. At a low E_b/N_0, the iterative trajectory of the SI-BSIC-SFDE doesn't progress with more turbo iterations, despite a wide tunnel. In summary, the EXIT chart results match the correlation results in Fig. 5.

2) BIT ERROR RATE (BER) PERFORMANCE

For QPSK transmissions over the Proakis-C, MD-6 and MD-8 channels, BER performances of turbo equalization schemes with different soft equalizers are compared in Fig. 7, where the matched filter bound (MFB) is also included as

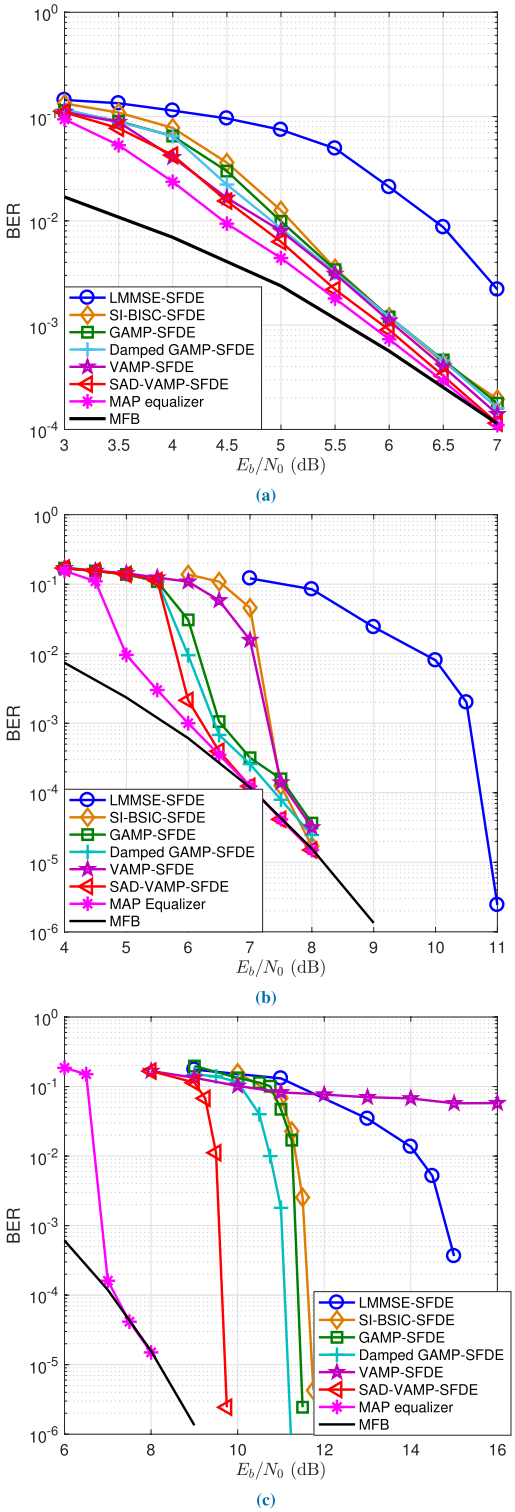

FIGURE 7. BER performance comparison among different turbo equalization schemes under (a) the Proakis-C channel, (b) the MD-6 channel, and (c) the MD-8 channel.

a performance reference. In particular, turbo equalization employing the damped GAMP-SFDE [37] is also included for comparison. The damped GAMP-SFDE is achieved by

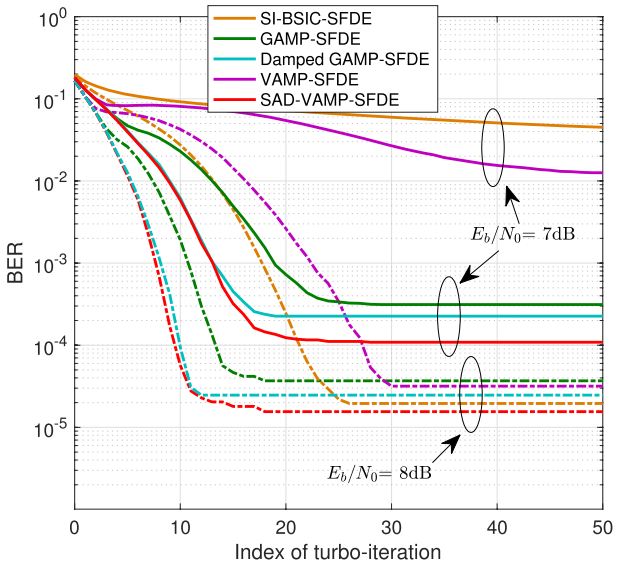

FIGURE 8. Convergence comparison among the SAD-VAMP-SFDE, VAMP-SFDE, damped GAMP-SFDE, GAMP-SFDE, and the SI-BSIC-SFDE under the MD-6 channel.

changing lines 2 and 8 of Algorithm 2 as follows

$$[\widehat{\mathbf{x}}_{1,k}]_n = \theta_{\mathrm{G}}\Big(\sum_{i=1}^{2^M}\alpha_i P(x_n=\alpha_i)\Big) + (1-\theta_{\mathrm{G}})[\widehat{\mathbf{x}}_{1,k-1}]_n \quad (11)$$

$$\mathbf{e}_{k+1} = \theta_{\mathrm{G}}\gamma_w(\mathbf{z} - \mathbf{S}\mathbf{F}\widehat{\mathbf{x}}_{2,k}) + (\mathbf{I} - \theta_{\mathrm{G}}\boldsymbol{\nu}_k)\mathbf{e}_k, \quad (12)$$

where the damping factor θ_{G} is chosen as $\theta_{\mathrm{G}} = 0.98\sqrt{4/\kappa}$, with κ being the peak-to-average ratio of $\mathbf{s}$ [37]. The number of inner iterations was set to 4 for the three SISEs, and the number of outer turbo iterations was 50.

Obviously, turbo equalization using SISEs significantly outperforms that using the LMMSE-SFDE in general. The proposed SAD-VAMP-SFDE consistently performs best among all SISEs, despite the channel condition. The VAMP-SFDE performs well under the Proakis-C channel while suffers performance divergence with the MD-8 channel. The divergence has already been observed in Fig. 3(d) and it is caused by the inaccurate extrinsic information exchanged between the ISS and ISE due to the violation of the right-rotationally invariant requirement under severe channels. The damped GAMP-SFDE achieves consistent performance gain over the original GAMP-SFDE.

In Fig. 8, the BERs are plotted as a function of the number of turbo iterations to compare the convergence speed. Clearly, at the same SNR condition, the SAD-VAMP-SFDE converges faster than other SISEs. This observation indicates the SAD-VAMP-SFDE excels also in the convergence speed in addition to the performance.

Last, the impact of the self-iteration number on the performance of the VAMP-SFDE and SAD-VAMP-SFDE based turbo equalization schemes is demonstrated in Fig. 9, where the MD-6 channel has been simulated. For the VAMP-SFDE, the turbo equalization performance nevertheless decreases as the self iteration continues over the low E_b/N_0 region,

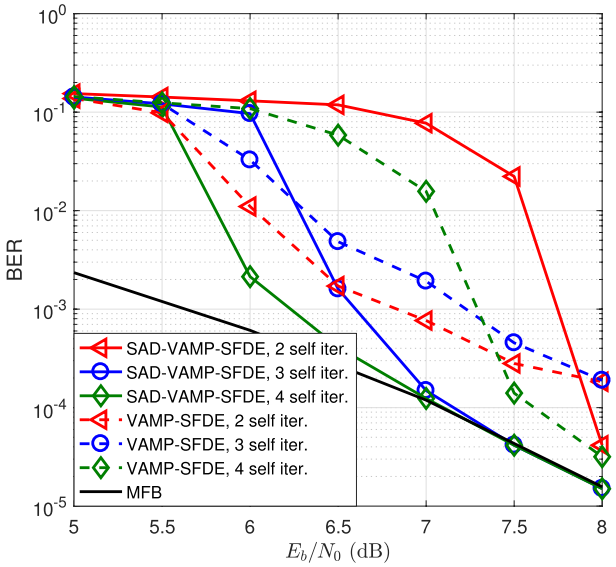

FIGURE 9. Demonstration of the self-iterative number on the performances of VAMP-SFDE and SAD-VAMP-SFDE based turbo equalization schemes.

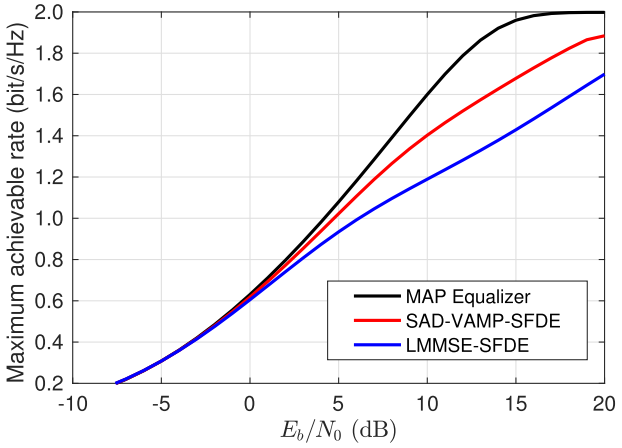

FIGURE 10. Maximum achievable rate versus E_b/N_0 for different soft equalizers under the MD-6 channel (QPSK modulation).

which coincides with the result in Fig. 3(c). With the help of the SAD, the performance of the SAD-VAMP-SFDE based turbo equalization keeps improving with the self-iteration number, verifying the effectiveness of self-iterative mechanism for a soft equalizer.

IV. NEAR-CAPACITY TRANSCEIVER DESIGN BASED ON THE SAD-VAMP-SFDE

The SAD-VAMP-SFDE has proved to be a preferred SISE for practical use. In this section, a near-capacity transceiver design is proposed and it adopts the SAD-VAMP-SFDE based turbo equalization on the receiver side.

Let $I_{\text{out}}^D = T_D(I_{\text{in}}^D)$ denote the EXIT equation of a soft decoder. According to the rate property [43], the rate of the channel code is approximated by

$$R_C \approx \int_0^1 T_D^{-1}(i)\mathrm{d}i = 1 - \int_0^1 T_D(i)\mathrm{d}i = 1 - A_D, \quad (13)$$

where $T_D^{-1}(i)$ is the inverse of $T_D(i)$ and A_D indicates the area under $I_{\text{out}}^D = T_D(I_{\text{in}}^D)$ in an EXIT chart. Similarly, let $I_{\text{out}}^E = T_E(I_{\text{in}}^E, E_b/N_0)$ denote the EXIT equation of a soft equalizer and the area under this EXIT curve is $A_E = \int_0^1 T_E(i, E_b/N_0)\mathrm{d}i$. When $R_C < A_E$, it is possible to achieve error-free transmission at an information rate up to [32], [40]

$$R_{\max}(E_b/N_0) \approx M \cdot A_E \quad [\text{bit/s/Hz}], \quad (14)$$

where the constellation parameter M denotes the number of bits per symbol. In Fig. 10, $R_{\max}$ curves as a function of E_b/N_0 for the SAD-VAMP-SFDE and the LMMSE-SFDE under the MD-6 channel with QPSK modulation are shown, and the result for the optimal MAP equalizer is also included as the approximate uniform input capacity [32], [44] of the MD-6 channel. From the figure, for a target maximum information rate of 1 bit/s/Hz, the SAD-VAMP-SFDE based iterative receiver is only 0.5 dB away from an optimal MAP receiver.

Next, we focus on the design of a rate-$\frac{1}{2}$ channel code for a system employing QPSK modulation with the assumption that the symbol rate equals to the bandwidth. We start the discussion by first introducing a unity-rate code (URC) between the channel encoder and the constellation mapping. The purpose is to make the EXIT curve of the combination of the SAD-VAMP-SFDE and URC decoder approach (1, 1) point, such that the performance of the channel decoding can be maximized.

A. URC PRECODING

As shown in Fig. 6(d), the endpoint of the SAD-VAMP-SFDE EXIT curve cannot reach the (1, 1) point under the MD-6 channel at a low SNR. This is due to the finite memory of the ISI channel, which leads to a poor distance spectrum affecting the decoding performance [1]. This fact motivates us to introduce a precoder with infinite memory between the channel encoder and the ISI channel so as to improve the distance spectrum. A URC with generator polynomial $G(D) = 1/(1 + D)$ was chosen. An interleaver (Π_2) for randomizing the extrinsic outputs of the URC decoder was placed between the URC encoder and the constellation mapper, leading to a transmitter design shown in the upper half of Fig. 11. Corresponding to such a transmitter design, a three-fold iterative receiver system [40], [45] as shown in the bottom half of Fig. 11, is adopted. The inner two-fold iterative subsystem made up of the SAD-VAMP-SFDE and the URC decoder is named the SAD-VAMP-SFDE-plus-URCD. The EXIT curves of the SAD-VAMP-SFDE-plus-URCD at E_b/N_0 of 5.2 dB and 6.0 dB are shown in Fig. 12, where the number of iterations between the SAD-VAMP-SFDE and the URC decoder was set to 3. At $E_b/N_0 = 5.2$ dB, $A_E = 0.5138$ which is barely larger than the coding rate 0.5 so it is theoretically possible to achieve error-free detection if the channel coding is properly designed.

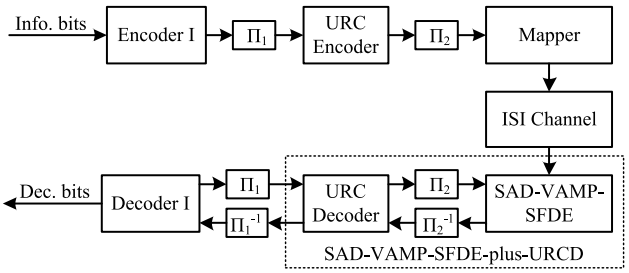

FIGURE 11. Block diagram of the proposed transceiver system.

B. MATCHING IRREGULAR RECURSIVE CONVOLUTIONAL CODE

To approach the capacity, the irregular convolutional code (IrCC) is chosen as it can adjust the shape of its EXIT curve to match that of the SAD-VAMP-SFDE-plus-URCD in turbo equalization. The IrCCs have been widely used in many applications including the near-capacity MMSE turbo equalization [45], [46], cooperative multi-user communications [47], and space-time block code designs [48], [49], etc.

The IrCC is designed as a weighted combination of a set of 17 subcodes with different rates. The k-th subcode has a coding rate $r_k = 0.1 + (k-1) \times 0.05$ and a weighting coefficient $\omega_k \in [0, 1]$. Given a target rate R_C^{IrCC}, the following equality shall be met

$$\sum_{k=1}^{17} \omega_k r_k = R_C^{\text{IrCC}} \text{ s.t.} \sum_{k=1}^{17} \omega_k = 1. \tag{15}$$

At $E_b/N_0 = 5.2$ dB and $R_C^{\text{IrCC}} = 0.5$, the optimal weight coefficients are solved [32] as

$$\begin{aligned}[\omega_1, \omega_2, \ldots, \omega_{17}] \\ = [&0.1424, 0.1404, 0, 0.0859, 0, 0.0813, \\ &0.0427, 0.0119, 0.0375, 0.0067, \\ &0.0706, 0, 0, 0.0982, 0, 0, 0.2824].\end{aligned} \tag{16}$$

The EXIT curve of the matched IrCC is plotted in Fig. 12, where the tunnel between the SAD-VAMP-SFDE-plus-URCD EXIT curve at $E_b/N_0 = 5.2$ dB and the IrCC EXIT curve is very slim as expected. Due to the length limitation of the interleavers (2^{15} bits for both Π_1 and Π_2) leading to non-Gaussian distributed *a priori* LLRs [40], [50], the actual trajectory does not pass the tunnel at $E_b/N_0 = 5.2$ dB. Instead, the trajectory at a higher E_b/N_0 of 6 dB is shown in Fig. 12. Obviously, it converges to the (1, 1) point, despite a deviation from the EXIT curves.

C. PERFORMANCE

The performance of the proposed system with three-fold iterative receiver scheme in Fig. 11 was investigated and compared with the original system with two-fold iterative receiver in section III. For the simulations, the MD-6 channel and QPSK modulation were adopted and the maximum number of the turbo iterations was set as 50. The results are

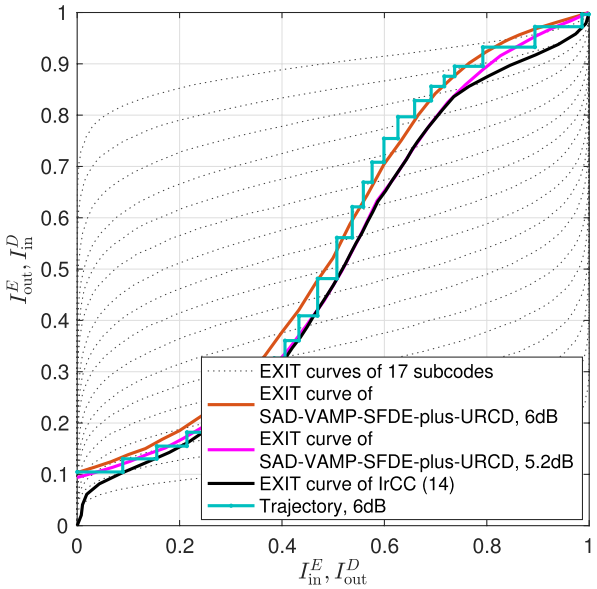

FIGURE 12. EXIT chart of the three-fold iterative receiver (EXIT curves of the 17 subcodes are shown in the background).

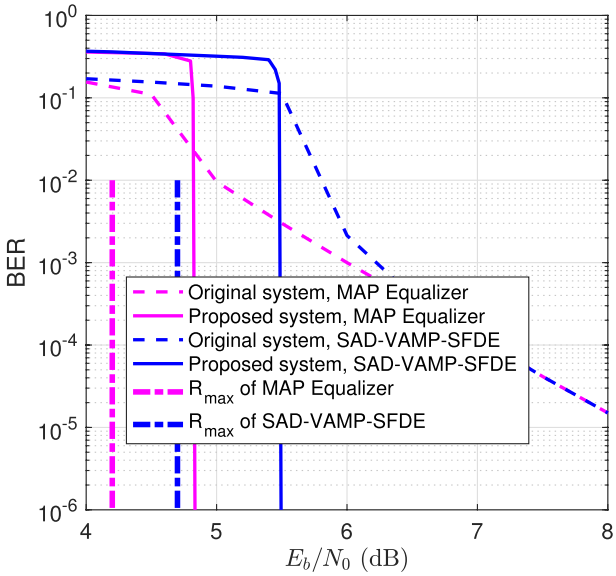

FIGURE 13. BER performance comparison between the proposed transmission system and the original transmission system.

shown in Fig. 13, where the performance of a near-capacity transceiver system obtained by replacing the SAD-VAMP-SFDE with the optimal MAP equalizer in Fig. 11 is also included as a reference. From the figure, the performance gain of proposed system over the original system was obvious attributed to the specifically designed URC and IrCC. At the BER level of 10^{-5}, the proposed systems adopting the MAP equalizer and the SAD-VAMP-SFDE are 0.65 dB and 0.80 dB away from their approximate uniform input capacities, respectively. The performance loss is due to the gap between the matched IrCC and a perfect channel coding [51] as well as the limited interleaver lengths [40], [50].

In summary, the proposed system with the SAD-VAMP-SFDE is only 1.3 dB from the approximate uniform input capacity achieved via an ideal channel coding and the MAP equalizer.

V. CONCLUSION

The self-iterative vector approximate message passing (VAMP) soft frequency-domain equalizer (SFDE) was revisited. First, it was compared with other self-iterative soft equalizers (SISEs), including the self-iterative block-wise soft interference cancellation (SI-BSIC) SFDE and the generalized approximate message passing (GAMP) SFDE. It was shown the SI-BSIC-SFDE is a simplified variant of the VAMP-SFDE and the GAMP-SFDE has a similar structure to the VAMP-SFDE except for the Onsager correction term in the extrinsic information computation. In terms of complexity, the VAMP-SFDE is comparable to the other two SISEs. Second, state evolution (SE) analysis was performed for the VAMP-SFDE, and it led to an improved semi-adaptive damping (SAD) setting. The resulting SAD-VAMP-SFDE together with the GAMP-SFDE and SI-BSIC-SFDE, were then compared via EXIT chart analysis and bit error rate (BER) within the scope of turbo equalization. Under highly frequency-selective channels, the proposed SAD-VAMP-SFDE outperforms the other SISEs and approaches the matched filter bound (MFB) over lower SNR region. Last, a near-capacity transceiver scheme was proposed. It included a URC precoding in addition to a matching IrCC channel coding at the transmitter and employed a three-fold iterative detection scheme on the receiver side. It achieved considerable performance gain over a transmission system without specific design of the channel coding.

REFERENCES

[1] M. Tüchler and A. C. Singer, "Turbo equalization: An overview," *IEEE Trans. Inf. Theory*, vol. 57, no. 2, pp. 920–952, Feb. 2011.

[2] Y. Li, B. Vucetic, and Y. Sato, "Optimum soft-output detection for channels with intersymbol interference," *IEEE Trans. Inf. Theory*, vol. 41, no. 3, pp. 704–713, May 1995.

[3] X. Wang and H. V. Poor, "Iterative (turbo) soft interference cancellation and decoding for coded CDMA," *IEEE Trans. Commun.*, vol. 47, no. 7, pp. 1046–1061, Jul. 1999.

[4] M. Tüchler, A. C. Singer, and R. Koetter, "Minimum mean squared error equalization using *a priori* information," *IEEE Trans. Signal Process.*, vol. 50, no. 3, pp. 673–683, Mar. 2002.

[5] J. Tao, "On low-complexity soft-input soft-output linear equalizers," *IEEE Wireless Commun. Lett.*, vol. 5, no. 2, pp. 132–135, Apr. 2016.

[6] Q. Guo and D. D. Huang, "A concise representation for the soft-in soft-out LMMSE detector," *IEEE Commun. Lett.*, vol. 15, no. 5, pp. 566–568, May 2011.

[7] J. Tao, "Single-carrier frequency-domain turbo equalization with various soft interference cancellation schemes for MIMO systems," *IEEE Trans. Commun.*, vol. 63, no. 9, pp. 3206–3217, Sep. 2015.

[8] J. Tao, "On low-complexity soft-input soft-output decision-feedback equalizers," *IEEE Commun. Lett.*, vol. 20, no. 9, pp. 1737–1740, Sep. 2016.

[9] J. Tao, J. Wu, Y. R. Zheng, and C. Xiao, "Enhanced MIMO LMMSE turbo equalization: Algorithm, simulations, and undersea experimental results," *IEEE Trans. Signal Process.*, vol. 59, no. 8, pp. 3813–3823, Aug. 2011.

[10] N. Benvenuto and S. Tomasin, "Iterative design and detection of a DFE in the frequency domain," *IEEE Trans. Commun.*, vol. 53, no. 11, pp. 1867–1875, Nov. 2005.

[11] N. Benvenuto, R. Dinis, D. Falconer, and S. Tomasin, "Single carrier modulation with nonlinear frequency domain equalization: An idea whose time has come—Again," *Proc. IEEE*, vol. 98, no. 1, pp. 69–96, Jan. 2010.

[12] D. L. Donoho, A. Maleki, and A. Montanari, "Message-passing algorithms for compressed sensing," *Proc. Nat. Acad. Sci. USA*, vol. 106, no. 45, pp. 18914–18919, Nov. 2009.

[13] D. L. Donoho, A. Maleki, and A. Montanari, "Message passing algorithms for compressed sensing: I. Motivation and construction," in *Proc. IEEE Inf. Theory Workshop Inf. Theory (ITW)*, Jan. 2010, pp. 1–5.

[14] S. Rangan. (2010). "Generalized approximate message passing for estimation with random linear mixing." [Online]. Available: https://arxiv.org/abs/1010.5141

[15] S. Rangan, "Generalized approximate message passing for estimation with random linear mixing," in *Proc. IEEE Int. Symp. Inf. Theory (ISIT)*, Jul./Aug. 2011, pp. 2168–2172.

[16] M. Bayati and A. Montanari, "The dynamics of message passing on dense graphs, with applications to compressed sensing," *IEEE Trans. Inf. Theory*, vol. 57, no. 2, pp. 764–785, Feb. 2011.

[17] Q. Guo, D. Huang, S. Nordholm, J. Xi, and Y. Yu, "Iterative frequency domain equalization with generalized approximate message passing," *IEEE Signal Process. Lett.*, vol. 20, no. 6, pp. 559–562, Jun. 2013.

[18] Y. Zhao, Y. Xiao, P. Yang, B. Dong, R. Shi, and K. Deng, "Generalized approximate message passing aided frequency domain turbo equalizer for single-carrier spatial modulation," *IEEE Trans. Veh. Technol.*, vol. 67, no. 4, pp. 3630–3634, Apr. 2018.

[19] Q. Shi, N. Wu, X. Ma, and H. Wang, "Frequency-domain joint channel estimation and decoding for faster-than-nyquist signaling," *IEEE Trans. Commun.*, vol. 66, no. 2, pp. 781–795, Feb. 2018.

[20] A. T. Abebe and C. G. Kang, "Iterative decoders for FTN-based NOMA scheme to multiplex sporadic and broadband transmission," in *Proc. Int. Conf. Inf. Commun. Technol. Converg. (ICTC)*, Oct. 2018, pp. 813–817.

[21] Q. Guo and J. Xi. (2015). "Approximate message passing with unitary transformation." [Online]. Available: https://arxiv.org/abs/1504.04799

[22] S. Rangan, P. Schniter, and A. K. Fletcher. (2016). "Vector approximate message passing." [Online]. Available: https://arxiv.org/abs/1610.03082

[23] S. Rangan, P. Schniter, and A. K. Fletcher, "Vector approximate message passing," in *Proc. IEEE Int. Symp. Inf. Theory (ISIT)*, Jun. 2017, pp. 1588–1592.

[24] J. Ma and L. Ping, "Orthogonal AMP," *IEEE Access*, vol. 5, pp. 2020–2033, 2017.

[25] K. Takeuchi, "Rigorous dynamics of expectation-propagation-based signal recovery from unitarily invariant measurements," in *Proc. IEEE Int. Symp. Inf. Theory (ISIT)*, Jun. 2017, pp. 501–505.

[26] P. Sun, C. Zhang, Z. Wang, C. N. Manchón, and B. H. Fleury, "Iterative receiver design for ISI channels using combined belief- and expectation-propagation," *IEEE Signal Process. Lett.*, vol. 22, no. 10, pp. 1733–1737, Oct. 2015.

[27] S. Şahin, A. M. Cipriano, C. Poulliat, and M.-L. Boucheret, "Iterative equalization with decision feedback based on expectation propagation," *IEEE Trans. Commun.*, vol. 66, no. 10, pp. 4473–4487, Oct. 2018.

[28] S. Şahin, A. M. Cipriano, C. Poulliat, and M.-L. Boucheret, "A framework for iterative frequency domain EP-based receiver design," *IEEE Trans. Commun.*, vol. 66, no. 12, pp. 6478–6493, Dec. 2018.

[29] I. Santos, J. J. Murillo-Fuentes, R. Boloix-Tortosa, E. Arias-de-Reyna, and P. M. Olmos, "Expectation propagation as turbo equalizer in ISI channels," *IEEE Trans. Commun.*, vol. 65, no. 1, pp. 360–370, Jan. 2017.

[30] I. Santos, J. J. Murillo-Fuentes, E. Arias-de-Reyna, and P. M. Olmos, "Turbo EP-based equalization: A filter-type implementation," *IEEE Trans. Commun.*, vol. 66, no. 9, pp. 4259–4270, Sep. 2018.

[31] J. Céspedes, P. M. Olmos, M. Sánchez-Fernández, and F. Perez-Cruz, "Probabilistic MIMO symbol detection with expectation consistency approximate inference," *IEEE Trans. Veh. Technol.*, vol. 67, no. 4, pp. 3481–3494, Apr. 2018.

[32] M. Tüchler, "Design of serially concatenated systems depending on the block length," *IEEE Trans. Commun.*, vol. 52, no. 2, pp. 209–218, Feb. 2004.

[33] C. Berrou, A. Glavieux, and P. Thitimajshima, "Near Shannon limit error-correcting coding and decoding: Turbo-codes. 1," in *Proc. IEEE Int. Conf. Commun. (ICC)*, Geneva, Switzerland, vol. 2, May 1993, pp. 1064–1070.

[34] F. Magee and J. Proakis, "An estimate of the upper bound on error probability for maximum-likelihood sequence estimation on channels having a finite-duration pulse response (Corresp.)," *IEEE Trans. Inf. Theory*, vol. IT-19, no. 5, pp. 699–702, Sep. 1973.

[35] S. T. Brink, "Convergence behavior of iteratively decoded parallel concatenated codes," *IEEE Trans. Commun.*, vol. 49, no. 10, pp. 1727–1737, Oct. 2001.
[36] S. T. Brink, G. Kramer, and A. Ashikhmin, "Design of low-density parity-check codes for modulation and detection," *IEEE Trans. Commun.*, vol. 52, no. 4, pp. 670–678, Apr. 2004.
[37] S. Rangan, P. Schniter, and A. Fletcher, "On the convergence of approximate message passing with arbitrary matrices," in *Proc. IEEE Int. Symp. Inf. Theory (ISIT)*, Jun./Jul. 2014, pp. 236–240.
[38] F. Caltagirone, L. Zdeborová, and F. Krzakala, "On convergence of approximate message passing," in *Proc. IEEE Int. Symp. Inf. Theory (ISIT)*, Jun./Jul. 2014, pp. 1812–1816.
[39] J. Vila, P. Schniter, S. Rangan, F. Krzakala, and L. Zdeborová, "Adaptive damping and mean removal for the generalized approximate message passing algorithm," in *Proc. IEEE Int. Conf. Acoust., Speech Signal Process. (ICASSP)*, Apr. 2015, pp. 2021–2025.
[40] M. El-Hajjar and L. Hanzo, "EXIT charts for system design and analysis," *IEEE Commun. Surveys Tuts.*, vol. 16, no. 1, pp. 127–153, 1st, Quart. 2014.
[41] S. Jeong and J. Moon, "Self-iterating soft equalizer," *IEEE Trans. Commun.*, vol. 61, no. 9, pp. 3697–3709, Sep. 2013.
[42] J. Hokfelt, O. Edfors, and T. Maseng, "Turbo codes: Correlated extrinsic information and its impact on iterative decoding performance," in *Proc. IEEE 49th Veh. Technol. Conf.*, vol. 3, May 1999, pp. 1871–1875.
[43] J. Hagenauer, "The EXIT chart—Introduction to extrinsic information transfer in iterative processing," in *Proc. 12th Eur. Signal Process. Conf.*, Sep. 2004, pp. 1541–1548.
[44] D. M. Arnold, H.-A. Loeliger, P. O. Vontobel, A. Kavčić, and W. Zeng, "Simulation-based computation of information rates for channels with memory," *IEEE Trans. Inf. Theory*, vol. 52, no. 8, pp. 3498–3508, Aug. 2006.
[45] J. Wang, S. X. Ng, A. Wolfgang, L. L. Yang, S. Chen, and L. Hanzo, "Near-capacity three-stage MMSE turbo equalization using irregular convolutional codes," in *Proc. 4th Int. Symp. Turbo Codes Rel. Topics*, Apr. 2006, pp. 1–6.
[46] M. Grossmann, "Outage performance analysis and code design for three-stage MMSE turbo equalization in frequency-selective Rayleigh fading channels," *IEEE Trans. Veh. Technol.*, vol. 60, no. 2, pp. 473–484, Feb. 2011.
[47] H. V. Nguyen, S. X. Ng, J. L. Rebelatto, Y. Li, and L. Hanzo, "Near-capacity network coding for cooperative multi-user communications," in *Proc. IEEE Veh. Technol. Conf.*, Sep. 2011, pp. 1–5.
[48] L. Kong, S. X. Ng, R. G. Maunder, and L. Hanzo, "Irregular distributed space-time code design for near-capacity cooperative communications," in *Proc. IEEE 70th Veh. Technol. Conf. Fall*, Sep. 2010, pp. 1–6.
[49] H. V. Nguyen, C. Xu, S. X. Ng, and L. Hanzo, "Near-capacity wireless system design principles," *IEEE Commun. Surveys Tuts.*, vol. 17, no. 4, pp. 1806–1833, 4th Quart., 2015.
[50] R. Y. S. Tee, R. G. Maunder, and L. Hanzo, "EXIT-chart aided near-capacity irregular bit-interleaved coded modulation design," *IEEE Trans. Wireless Commun.*, vol. 8, no. 1, pp. 32–37, Jan. 2009.
[51] L. Kong, S. X. Ng, R. Y. S. Tee, R. G. Maunder, and L. Hanzo, "Reduced-complexity near-capacity downlink iteratively decoded generalized multilayer space-time coding using irregular convolutional codes," *IEEE Trans. Wireless Commun.*, vol. 9, no. 2, pp. 684–695, Feb. 2010.

DONG LI received the B.S. degree in underwater acoustic engineering from Harbin Engineering University, Harbin, China, in 2016. He is currently pursuing the Ph.D. degree with the Institute of Acoustics, Chinese Academy of Sciences, Beijing, China. His research interests include wireless and underwater acoustic communication, including turbo equalization, channel estimation, and underwater acoustic signal processing.

YANBO WU received the B.S. and Ph.D. degrees in electronic engineering from the Beijing Institute of Technology, Beijing, China, in 2003 and 2008, respectively. Since 2008, he has been with the Institute of Acoustics, Chinese Academy of Sciences, Beijing, where he is currently a Professor with the Ocean Acoustic Technology Center. He has authored or coauthored more than 30 journal and conference papers, and holds four patents. His research interests include turbo equalization, channel codes, and underwater acoustic communications.

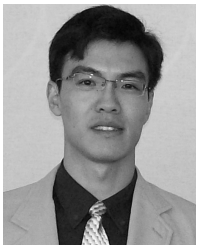

JUN TAO (S'10–M'10) received the B.S. and M.S. degrees in electrical engineering from the Department of Radio Engineering, Southeast University, Nanjing, China, in 2001 and 2004, respectively, and the Ph.D. degree in electrical engineering from the Department of Electrical and Computer Engineering, University of Missouri, Columbia, MO, USA, in 2010.

From 2004 to 2006, he was a System Design Engineer with Realsil Microelectronics, Inc., (a subsidiary of Realtek), Suzhou, China. From 2011 to 2015, he was a Senior System Engineer with Qualcomm, Inc., Boulder, CO, USA, involved in the baseband algorithm and architecture design for the UMTS/LTE modem. Since 2016, he has been a Full Professor with the School of Information Science and Engineering, Southeast University, Nanjing, China. His research interests include wireless cellular communications and underwater acoustic communications, including channel modeling and estimation, turbo equalization, adaptive filtering, and baseband algorithm design for practical systems conforming to the UMTS and LTE standards.

MIN ZHU received the B.S. degree from the University of Science and Technology of China, Hefei, China, in 1994, and the M.S. and Ph.D. degrees from the Graduate University of Chinese Academy of Sciences, Beijing, China, in 2001 and 2006, respectively. He is currently a Professor with the Institute of Acoustics, Chinese Academy of Sciences. He is one of the second batches of leading scientists for the Ten-Thousand Talents Project. His research interests include underwater acoustic communications and networks, acoustic Doppler velocimetry technology, underwater acoustic detection, and acoustic systems of underwater human occupied vehicles.